Energy calibration of the ATLAS Liquid Argon Forward Calorimeter

2008 JINST 3 P02002

(http://iopscience.iop.org/1748-0221/3/02/P02002)

PUBLISHED BY INSTITUTE OF PHYSICS PUBLISHING AND SISSA

RECEIVED: *November 13, 2007*
ACCEPTED: *January 9, 2008*
PUBLISHED: *February 6, 2008*

Energy calibration of the ATLAS Liquid Argon Forward Calorimeter

J.P. Archambault,[a] A. Artamonov,[b] M. Cadabeschi,[c] V. Epshteyn,[b] C. Galt,[c*] P. Gorbounov,[c†] L. Heelan,[a] M. Khakzad,[a‡] V. Khovanskiy,[b] P. Krieger,[c§] P. Loch,[d] F.G. Oakham,[a¶] R.S. Orr,[c] J. Rutherfoord,[d] A. Savine,[d] M. Schram,[a] P. Shatalov,[b] L. Shaver,[d‖] M. Shupe,[d] V. Strickland[a¶] and I. Tsukerman[b]

[a] *Physics Department, Carleton University Ottawa, Ontario, K1S 5B6, Canada*
[b] *ITEP Moscow, 117 259 Moscow, Russia*
[c] *Physics Department, University of Toronto, Toronto, Ontario, M5S 1A7, Canada*
[d] *Physics Department, University of Arizona, Tucson, Arizona, 85721, U.S.A.*
E-mail: krieger@physics.utoronto.ca

ABSTRACT: One of the two ATLAS Forward Calorimeters (FCal), consisting of three modules, one behind the other, was exposed to particle beams of known energies in order to obtain the energy calibration. The data were taken in the H6 beamline at CERN in the summer of 2003, using electron and hadron beams with energies from 10 to 200 GeV. The beam test setup and collected data samples are described in detail. Using data samples taken with a minimal amount of material upstream of the calorimeter, the FCal response to electrons and pions, as measured by the linearity and resolution as a function of energy, is extracted and compared to ATLAS performance requirements.

KEYWORDS: Cryogenic detectors; Calorimeters; Large detector systems for particle and astroparticle physics.

*Now at the US Patent and Trademark Office, Alexandria, Virginia, 22313, U.S.A.
†Permanent Address, ITEP, Moscow
‡Now at Dept. of Physics, St. Francis Xavier University, Antigonish, NS, B2G 2W5, Canada
§Corresponding author.
¶Also at TRIUMF, Vancouver, BC, V6T 2A3, Canada
‖Retired.

2008 JINST 3 P02002

Contents

2008 JINST 3 P02002

1. Introduction

ATLAS is one of the two general purpose detectors that will take data at the Large Hadron Collider (LHC) at CERN, where protons will collide nearly head-on with energies of 7 TeV, at a design luminosity of 10^{34} cm^{-2} s^{-1}. The energies and density of particles produced in these collisions are largest near the directions of the incident beams. This harsh environment close to the accelerator beam pipe places severe constraints on the detector elements designed to operate there.

An important design criterion for ATLAS is hermetic calorimetry. That is, the interaction region should be surrounded by calorimeters so no electrons, photons, or hadrons with significant transverse momentum can escape undetected. The ATLAS Forward Calorimeters (FCals) extend the calorimetric coverage from a pseudorapidity, $|\eta|$, of about 3.1 to 4.9 and therefore sit quite close to the beam pipe. At design luminosity, each LHC bunch crossing will produce an average of about 23 soft collisions which will deposit large amounts of energy in the forward calorimeters. The deposited power load and extreme radiation doses to the detector components limit the

choice of construction materials and constrain the design of the calorimeter. Furthermore, these minimum bias events will overlap events of interest, complicating the reconstruction and smearing the calorimeter energy and position measurements.

A design with a forward calorimeter far from the interaction region (about 15 m) was originally considered [1], to ameliorate the consequences of the large particle density and radiation dose. However, this would have created a region of pseudorapidity between the endcap and forward calorimeters where shower spreading, leakage, and absorption in support structures would have compromised the measurement of transverse momentum and exacerbated problems due to upstream material. Instead, a design was adopted that integrated the forward calorimeter into the existing Liquid Argon (LAr) endcap calorimeter design [2]. This had the advantage of allowing for common readout electronics, as well as providing shielding for the muon detectors at high $|\eta|$.

The ATLAS FCal has been designed to survive in the environment near the LHC beamline while providing good energy and position measurements for jets. A major objective of the forward calorimetry is physics with high missing transverse energy, E_T. Good determination of missing E_T requires hermetic calorimetry to minimize contributions from high energy jets that escape detection at low angles to the beamline. Another key part of the LHC experimental programme is the search for the Higgs boson. At low masses, just above the LEP limit of 114.4 GeV/c^2 [3], early discovery of the Higgs may come from searches for Higgs production via the Vector-Boson-Fusion (VBF) process, which is characterized by high energy forward jets. The ability to tag these jets is another important requirement on the forward calorimeter performance. We set the requirements for E_T resolution at $\Delta E_T/E_T < 10\%$ for $E_T > 25$ GeV. Below this threshold tagging jets are lost in the pileup when running at the design luminosity. This requirement implies that the FCal energy resolution and jet angle resolution must both be better than about 7%; at the highest values of $|\eta|$ it is the angular resolution that dominates. The requirements on the position resolution dictate the necessary readout granularity of the detector.

A good measurement of the missing E_T requires not just hermetic calorimetry with adequate energy resolution, but also an energy response in which non-Gaussian tails are small, to ensure that instrumental contributions to the missing E_T signal, due for instance to mismeasurement of large cross-section QCD processes, are small compared to the expected physics signals.

The location of the forward calorimeter within the ATLAS endcap cryostat is illustrated in figure 1. A cross-sectional view of the upper half of the forward calorimeter in this environment is shown in figure 2, which provides more detail on its position relative to the other endcap calorimeters, and shows some of the material located between the FCal front face and the ATLAS interaction point (IP). Each FCal consists of three modules, referred to as FCal1, FCal2 and FCal3. The FCal1, a copper module, is closest to the interaction point, at $z = 4709.9$ mm. Behind it are the FCal2 and FCal3, respectively, which are made mainly of tungsten in order to optimize shower containment in the available space and limit the transverse spread of hadronic showers. Behind the FCal3 is an un-instrumented plug made of a copper alloy, which provides additional shielding for the muon system. The ATLAS moderator shield (ATLAS JM shield), here marked as "Poly Shield", is designed to reduce albedo from the calorimeter back into the inner detector [4]. The FCal sits within a cylindrical support tube that has a cone shaped extension on the IP side that bolts to the face of the cryostat; this assembly forms a structural component of the endcap cryostat. A cryostat bulkhead made of about 5 cm of aluminum is located just in front of the FCal1. The JM shielding consists

2008 JINST 3 P02002

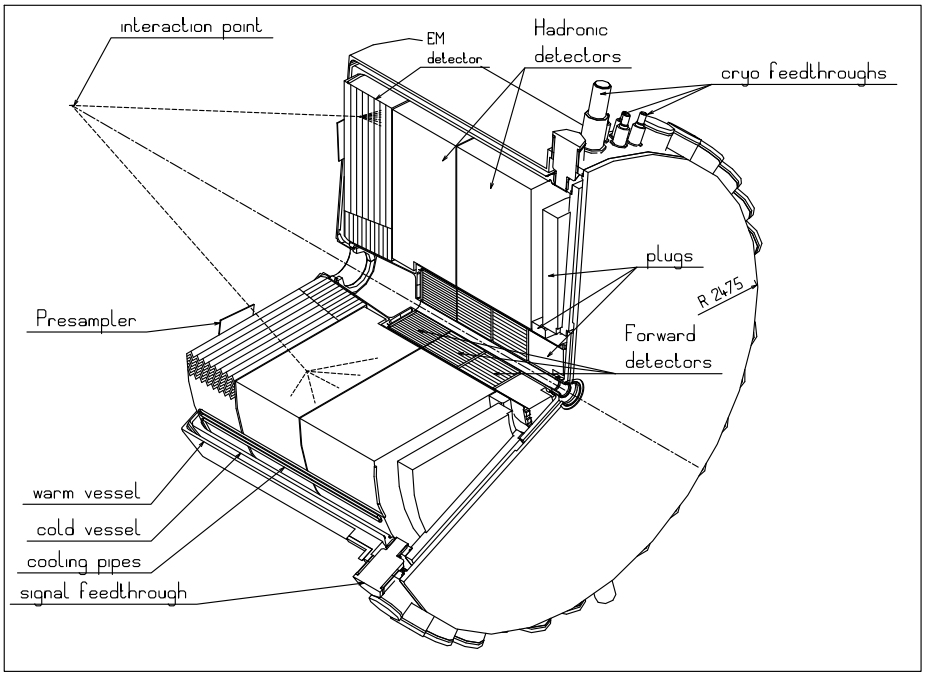

Figure 1. A cutaway view of the ATLAS endcap cryostat, showing the location of the forward calorimeter relative to the other endcap calorimeters [5].

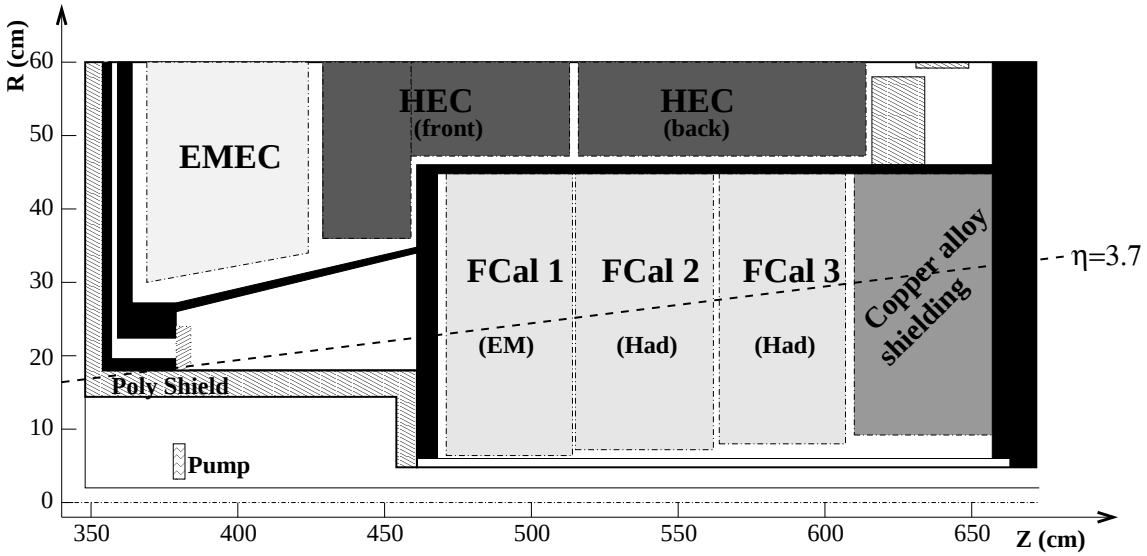

Figure 2. A cross-sectional view of the upper half of forward calorimeter, in the cryostat support tube which houses it; cryostat walls are shown in black. Particles at $|\eta| \approx 3.7$ (shown) must traverse both the the tube portion of the polyethylene shielding and the cryostat bulkhead. At higher $|\eta|$ there is additional material, for instance the plug portion of the Poly Shield as well as a metal pump, also illustrated.

of a tube of outer diameter 178.5 mm and 38.5 mm thickness, extending for just over a meter in front of the FCal, and an 80 mm thick plug with inner and outer radii of 74.5 mm and 178.5 mm,

2008 JINST 3 P02002

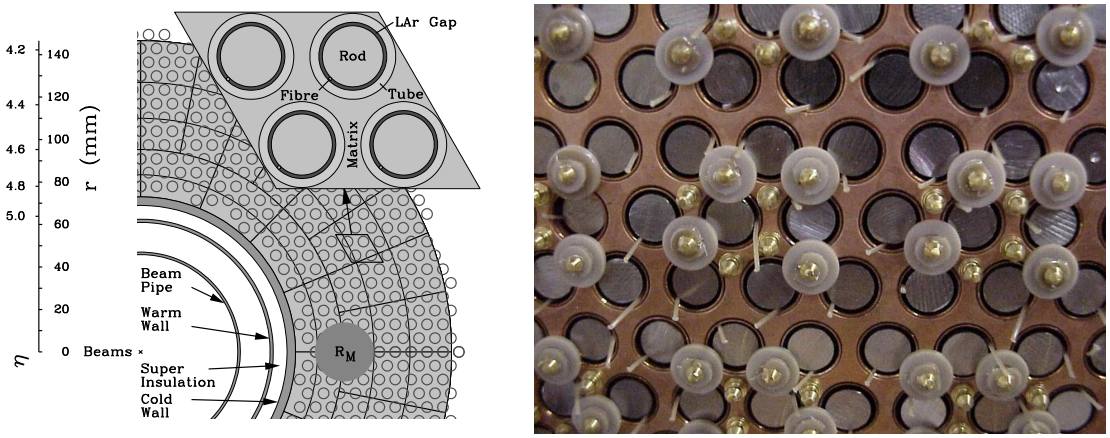

Figure 3. Forward calorimeter electrode arrangement. The left-hand plot shows a schematic view of a portion of the front face of the FCal1, also illustrating a single electrode group and indicating the size of the Molière radius in this device. The right-hand figure shows a photograph of the front (non-readout) face of a hadronic (FCal3) module. Also visible are PEEK retention washers, that keep the anode rods in position, and the ends of the PEEK fibres that maintain the narrow LAr gaps.

concentric with the beamline and situated just upstream of the cryostat bulkhead described above. Also illustrated in the figure is the material of a small pump that sits within the evacuated volume of the cone.

In order for the FCal to operate in the very high flux environment that will be present when the LHC is run at its design luminosity, the liquid argon gaps in the forward calorimeter must be much smaller than the 1-2 mm gap size that is traditional in a LAr device. This constraint is accommodated by the use of a novel design with thin annular LAr gaps oriented parallel to the beamline. Electrodes are formed by inserting an absorber rod, which serves as the anode, into a copper tube which acts as the cathode. The rod is positioned concentrically in the tube using a helically-wound radiation-hard plastic fibre (PEEK) that maintains the narrow LAr gap (250 μm in the FCal1) and electrically separates the anode and cathode. These electrodes are positioned in a hexagonal array within an absorber matrix. The electrode-to-electrode spacing is quite small, leading to a detector with a fine lateral segmentation that can be exploited in the shower shape reconstruction. The module structure is illustrated in figure 3, which shows a schematic partial view of the front face of the FCal1 module alongside a photo of the non-readout face of the FCal3 module. For high voltage distribution and readout, electrodes are ganged together in groups of 4, 6, or 9 on the FCal1, FCal2 and FCal3, respectively, using interconnect boards at the readout face of each calorimeter module. For most channels, four such groups are summed on a transformer summing board before the signals are sent to the cryogenic feedthrough. At the inner and outer periphery of each module, there are some channels for which no summing is performed. This will be discussed in the next section.

In this paper we describe the performance of one of the two final ATLAS forward calorimeters to single particles, i.e. electrons and pions, over the energy range of about 10-200 GeV. More information on the design of the Forward Calorimeter can be found in reference [5]. Details of the design and construction of the as-built detector will be the subject of a forthcoming publication.

2008 JINST 3 P02002

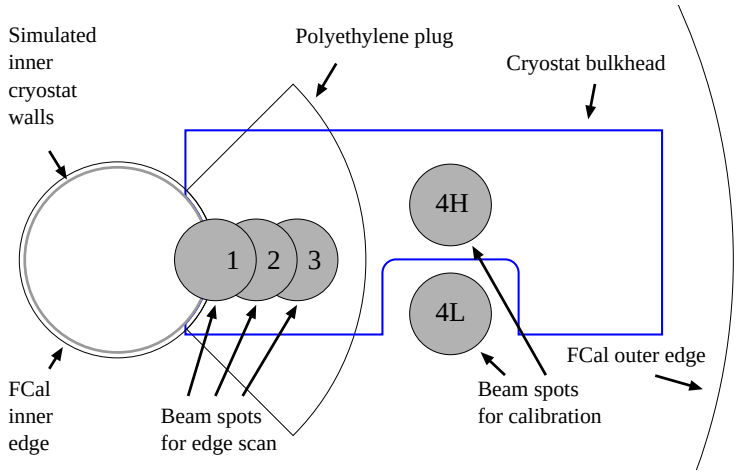

Point	angle	$\|\eta\|$
1	0.88°	4.9
2	1.25°	4.5
3	1.61°	4.3
4	2.98°	3.7

Figure 4. A view of the instrumented region of the FCal, showing the five impact points used in the beam test. Also shown are an aluminum plate used to simulated the cryostat bulkhead when running at the 4H position and a polyethylene piece simulating the plug part of the ATLAS JM moderator near the beam hole.

2. Beam test configuration

The aims of the 2003 beam test were two-fold: to determine the FCal energy calibration and to study its performance for particles near the inner radius of the detector, where leakage at the inner edge, or "splashing" across the beampipe must be understood. Several beam impact points were used, as shown in figure 4, and a wide (5 cm diameter) beam was chosen in order to average over the face of the calorimeter, since the FCal response is known to depend on the impact point relative to the closest electrode [6]. The two beam impact points used for the calibration energy scan (4H, 4L) differ in the amount of upstream material seen by the beam before reaching the calorimeter. At the 4L position, the amount of upstream material in front of the calorimeter was minimized in order to allow investigation of the intrinsic detector performance. At the 4H position, an attempt was made to simulate conditions at ATLAS, where particles at $|\eta| \approx 3.7$ must traverse a substantial amount of material before reaching the FCal, such as the cryostat bulkhead and the tube portion of the ATLAS JM shielding, which represents a large thickness of polyethylene at these incident angles. In ATLAS there will also be material associated with the inner detector and associated services. However, at the time of the beam test, the amount of material was not well known, and since it is expected to vary strongly with η and ϕ, no attempt was made to simulate it. This paper presents an analysis only of the data taken at the 4L position. Analysis of the other data samples will be the subject of future publications.

The original goal was to use a completed forward calorimeter installed in its support tube. However, delays in the availability of the tube made this impractical. Instead a purpose-built stand was constructed to hold the production modules of the forward calorimeter for the C-side of ATLAS. These were positioned with close-to-nominal spacing; the separations and any small relative rotations were surveyed after installation. Figure 5 shows a drawing of the three modules on the beam test stand and a photograph of the cabled modules inside the cryostat at CERN.

Because of the very narrow liquid argon gaps, high-voltage shorts in electrodes can be induced

2008 JINST 3 P02002

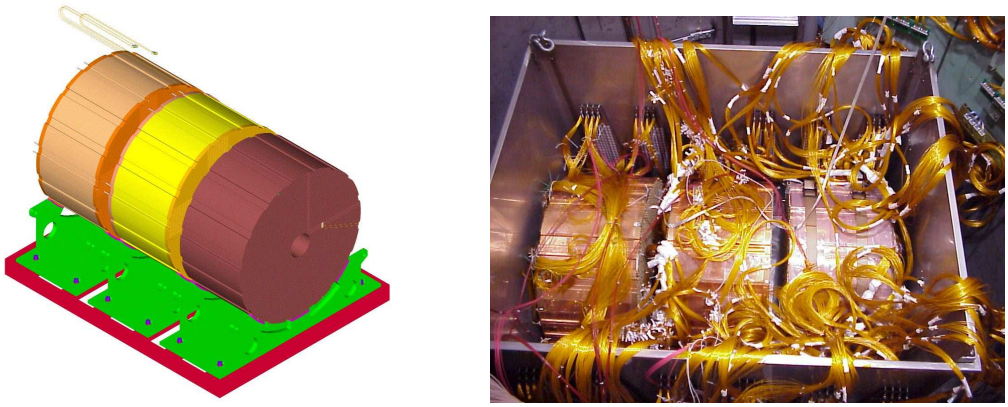

Figure 5. Module setup for the FCal beam test. The left-hand diagram shows a CAD drawing of the three FCal modules on the beam test stand. The right-hand figure shows an overhead view of the cabled modules inside the bathtub. Also visible, on the inner and outer walls of the bathtub, are some of the summing boards.

by rather small pieces of conductive material. Past experience with module cold tests done in the same cryostat led us to take measures to protect the modules against any debris left after cleaning of the cryostat. The detector stand, with the three modules installed, was therefore inserted into a "bathtub" made of 1.5 mm stainless steel. The bathtub had several holes covered in a fine stainless steel mesh to allow LAr flow into the bathtub during filling of the cryostat. The LAr fill was controlled to maintain a level below the top of the bathtub.

The cabling of each FCal module is segmented into 16 azimuthal (ϕ) slices. The readout of each ϕ slice is additionally segmented into 4 η regions in the FCal1, 2 in the FCal2 and 1 in the FCal3, with each region having it's own cable harness instrumenting up to 64 electrode groups. For most channels the signals from four electrode groups are summed by a transformer on a summing board located inside the cryostat. Each summing board receives four cable harnesses from the modules and outputs one "pigtail" cable carrying up to 64 readout channels from the summing board to the cryogenic signal feedthrough, as illustrated in figure 6. To accommodate the geometry at the inner and outer radii of the detector, some electrode groups in these regions are read out without summing. While the FCal modules were fully cabled prior to the beam tests, because of a lack of pigtail cables and readout electronics, the FCal was not fully instrumented for the beam test. In order to ensure that energy splashing across the beam hole could be detected during the inner edge scan, the innermost η region was cabled for all ϕ slices. For both the FCal1 and FCal2 modules, in addition to the annular region, four ϕ slices forming a 90° wedge about $\phi = 0$ were instrumented to form a region providing approximate lateral containment for electrons and pions in the region used for the energy scan. The FCal3 module was fully instrumented since each cable harness instruments the full η region of a single ϕ slice. The instrumented regions of the three FCal modules are illustrated in figure 7.

To allow for position scans, the cryostat sits on rails and is equipped for lateral translation. Scanning in the vertical direction was achieved by adjusting the current in the final bend magnet (B9) in the H6 beamline, which is located about 32 m upstream of the cryostat. These features allow for the selection of specific beam impact points on the calorimeter. The mean response

2008 JINST 3 P02002

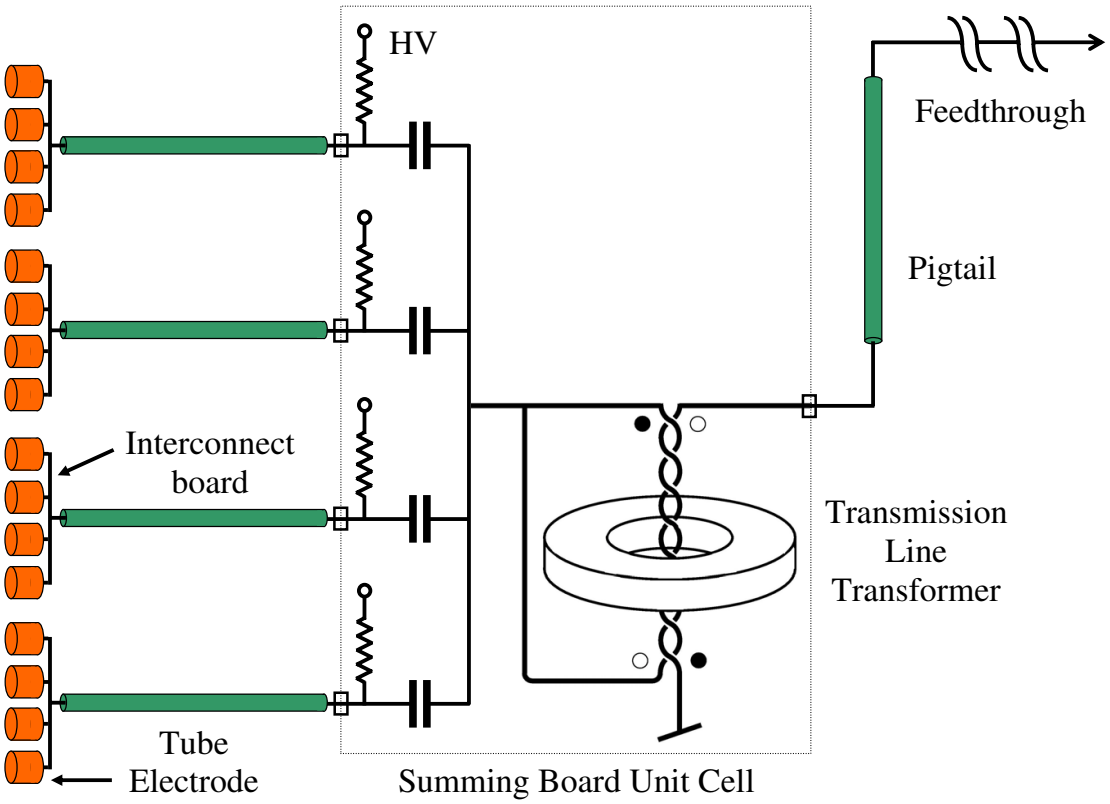

Figure 6. Schematic of the module cabling from the electrodes to the cryogenic feedthrough. Signals from four tube groups are summed on the transformer to produce a single "summed" channel which is then routed via the pigtail cables to the cryogenic feedthrough.

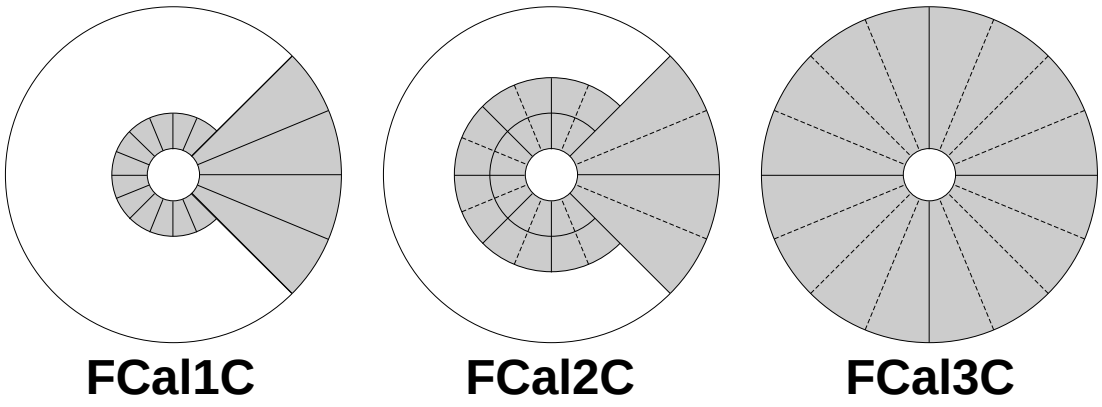

Figure 7. The shaded areas show the regions of the three FCal modules that were instrumented for the beam test. For the FCal1 and FCal2, the annular region ensures detection of any energy splashing across the beam-hole at points 1, 2 and 3, used for the inner edge scan, while the wedge shaped region provides for lateral containment at the points used for the energy calibration, which were indicated in figure 4.

of the forward calorimeter is known to depend on the particle impact point and the resolution is known to depend on the particle's impact angle. In order to run at each impact point with the same angle of incidence as would be the case at ATLAS, for particles originating from the interaction point, it was necessary to make mechanical modifications to the cryostat to also allow for small rotations. Changes from one impact point to another were accomplished by a combination of rotation and translation. The incident angles are summarized in figure 4. In the case of beams deflected vertically using the B9 magnet, the small additional contribution to the impact angle was not accounted for. Three vertical settings were used, one for the position scan points which were at the detector mid-plane and two for the energy scan, symmetrically located above (H) and below (L) the mid-plane.

For running at the 4H position and at the three positions used for the inner edge scan, we attempted to simulate, as much as was possible, an ATLAS-like environment. This meant modeling the cryostat bulkhead and the tube and plug portions of the ATLAS JM moderator. The tube region was modeled by placing polyethylene in the beamline upstream of the cryostat, in the slot of an iron wall located upstream of the cryostat, while the plug, relevant only for positions 1-3, was modeled with a polyethylene piece mounted to the outside of the front-face of the bathtub. The cryostat bulkhead was modeled using 5.0 cm of aluminum, bolted to the inside wall of the bathtub, with a cut-away around the 4L position. The material mounted on the bathtub wall is illustrated in figure 4. At position 1, the innermost scan point, we additionally modeled an ion pump that sits in the evacuated region of the forward cone, using a small aluminum block 30 mm thick placed in the beamline about 900 mm upstream of the detector.

A Rohacell excluder was placed between the inner wall of the cryostat and the outer wall of the bathtub. However, there was no excluder between the inner wall of the bathtub and the FCal1 front face, which was positioned 15 cm downstream of it. In the 4H position, 5 cm of this depth was occupied by the stainless steel plates used to model the cryostat bulkhead.

The liquid argon purity was monitored for the entire duration of the test, with oxygen contamination being less than 0.12 ppm at all times.

2.1 Beamline instrumentation

The beamline setup used for data-taking is illustrated in figure 8. The H6 beam emerges from a vertical bend magnet (B9) about 32 m upstream of the cryostat. There were three stations of Beam Positioning Chambers (BPCs), one located about 1 m downstream of the B9 magnet, one about 11 m downstream, and the third about 3 m upstream of the FCal, just in front of the cryostat. This last station was located on a movable table, described in more detail below. Each BPC station consisted of two *x*-plane and two *y*-plane MWPCs using delay line readout. The first and last stations provided hit resolution of 150-200 μm, while the middle station, which was of a somewhat older design, provided a hit resolution of about 300 μm. All BPCs had an efficiency near 100%. Information from the BPCs was used in the reconstruction of beam tracks, allowing determination of the particle impact point on the front face of the calorimeter.

The beamline contained several scintillators used for triggering. These were located on a movable table just in front of the cryostat, that was shifted up and down to follow the beam to the three vertical settings. There were two 10x10 cm scintillators, each 1 cm thick, denoted S1 and S2, respectively, and a smaller 7x7 cm scintillator, also 1 cm thick, denoted S3, located closest to the

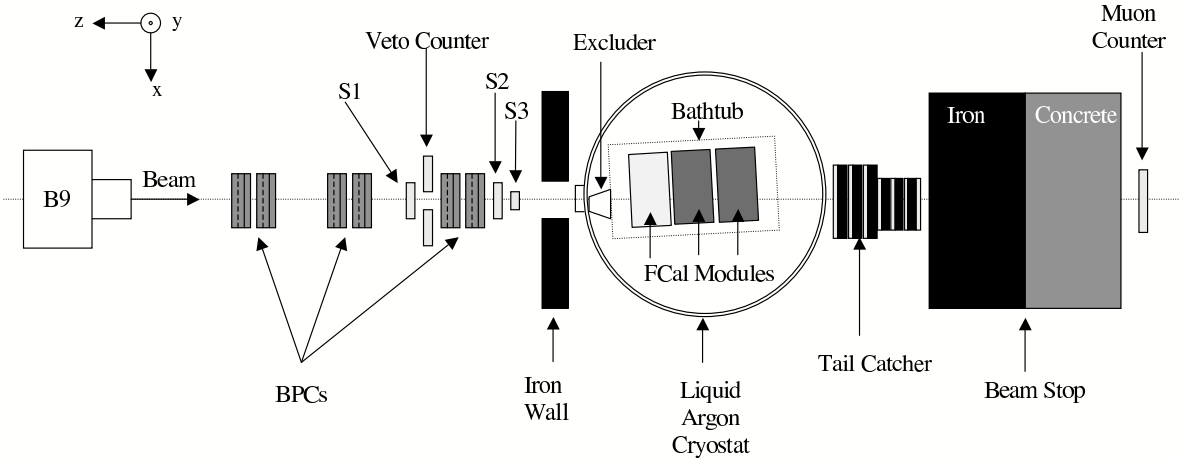

Figure 8. Schematic of the beamline setup for the FCal calibration beam test.

cryostat. There was also a veto counter made from a scintillator with a 6.5 cm diameter circular cut-out.

Downstream of the cryostat was a steel/scintillator tail-catcher, in the same configuration as was used in a 1998 beam test [6], with three thick scintillator plates of 140x140 cm^2 cross-sectional area followed by four 50x50 cm^2 counters. Each counter had two outputs with gain ratio of 1:28. Signals from the last two counters were summed to keep the number of readout channels matched to the number of inputs on a LeCroy 2249A ADC.

Downstream of the tail-catcher was a concrete beam stop, behind which was a 50x50 cm^2 muon counter. The aperture of this counter was insufficient to provide coverage for all scattered muons, especially at the lowest energies, so information from the tail-catcher is also required for the efficient suppression of muons.

Finally, for particle identification, a CEDAR [7] was located in the H6 beamline, upstream of the instrumentation illustrated in figure 8. This Čerenkov device can be used to distinguish electrons and pions at energies below about 100 GeV, and to provide pion-proton separation. The CEDAR contains eight photo-tubes and normally provides three coincidence signals, 6/8, 7/8 and 8/8 which were latched and written to the trigger word, event by event. However, only seven of the photo-tubes were functional during the period of this test. When CEDAR cuts are referred to in this paper, the requirement is the coincidence of 6 of the 7 functioning photo-tubes.

2.2 Module high voltage

The high voltage system used final ISEG FCal HV modules[1] and the associated crate and crate controller. These HV modules provide up to 600 V and 6 mA of current, with hardware interlocks adjustable by hand. A single supply houses two modules providing 8 channels each. Distribution of the HV to the calorimeter modules is done via the summing boards, as illustrated in figure 6. There are four independent HV lines per board, each serving one electrode group in each of the summed

[1]HV module ISEG EHS F006p_106_KB1, Iseg Spezialelektronik GmbH, Bautzener Landstr. 23, D-01454 Radeberg/Rossendorf. Manual to be found on [8].

2008 JINST 3 P02002

channels, as well as a fraction of the unsummed channels. In the case of a lost HV line, the resulting dead region is therefore distributed. Standard summing boards were used for all fully instrumented ϕ slices, but the cabling scheme described earlier required the construction of six special summing boards for the other instrumented regions. In total 16, summing boards were used, requiring 64 channels of HV, or four 16 channel supplies. A total of 994 readout channels were instrumented.

A great deal of effort went into development of FCal module assembly techniques that minimized the electrode failure rate due to HV shorts and great care was taken to minimize the exposure of the modules to debris during transportation and testing. During the construction and testing phases the electrode integrity was tested at various times, both warm and in liquid argon, in the same cryostat used for the beam test programme. These cold-tests showed the electrode failure rate to be less than 0.1%, meeting the design goal set for the production modules. However, these cold-tests were of limited duration, so the 2003 beam test additionally represented the longest test of the HV stability of the system, prior to the start of the LAr Calorimeter Endcap cold commissioning in 2007. From early on in the beam test there were five high voltage shorts present: one each in the FCal1 and FCal2, and three in the FCal3. Two additional shorts appeared in the FCal3 during the beam test programme.

2.3 Trigger and data acquisition system

Beam triggers were formed by a coincidence of the three beam counters S1, S2 and S3, with the Spill Gate, which was derived from the SPS accelerator clock and defined to exclude the very beginning and end of the spill, where unwanted spikes often occur. None of the other counters (Veto, CEDAR, Muon or Tail-catcher) were included into the trigger logic, in order to avoid undesirable systematic biases in the recorded data. Track selection and particle identification tasks ("beam cleaning") were allocated exclusively to the offline analysis.

In addition to the beam triggers, there were other types of events: start-of-burst and end-of-burst, random ("pedestal") triggers and calibration triggers (separately for the front-end electronics and the beam instrumentation). Burst events were used by the DAQ to synchronize the data taking and recording with the accelerator cycle. The calibration triggers for the beam instrumentation (MIPs for beam counters, time scale for the BPCs) were generated only at the start of each run, between the spills. Random trigger and front-end electronics calibration triggers were generated during the run, both during and between the spills. The relative rates of these triggers was tunable by software. The random triggers provided pedestal and noise measurements, while the front-end calibration triggers were passed to a special front-end calibration board, and used to determine the response of the Front End Boards (FEBs).

A trigger word was used to encode the information from the beam counters, to be used for fast offline event selection. This contained: three bits for the trigger counters; two bits (LatePU, EarlyPU) set for events that were too close in time, based on the logical sum of the S1, S2, S3 and Veto counters; two bits for the front and rear sections of the tail-catcher (with thresholds set well below the MIP peak); one bit each for the Muon and Veto counters; three bits for the CEDAR information; and one bit each for random and calibration triggers.

The beam test used prototypes of the ATLAS FEBs, close to the final design, with the readout following a chain similar to the one to be used in ATLAS. As illustrated in figure 6, signals from individual readout channels (summed or unsummed) are routed from the transformer summing

2008 JINST 3 P02002

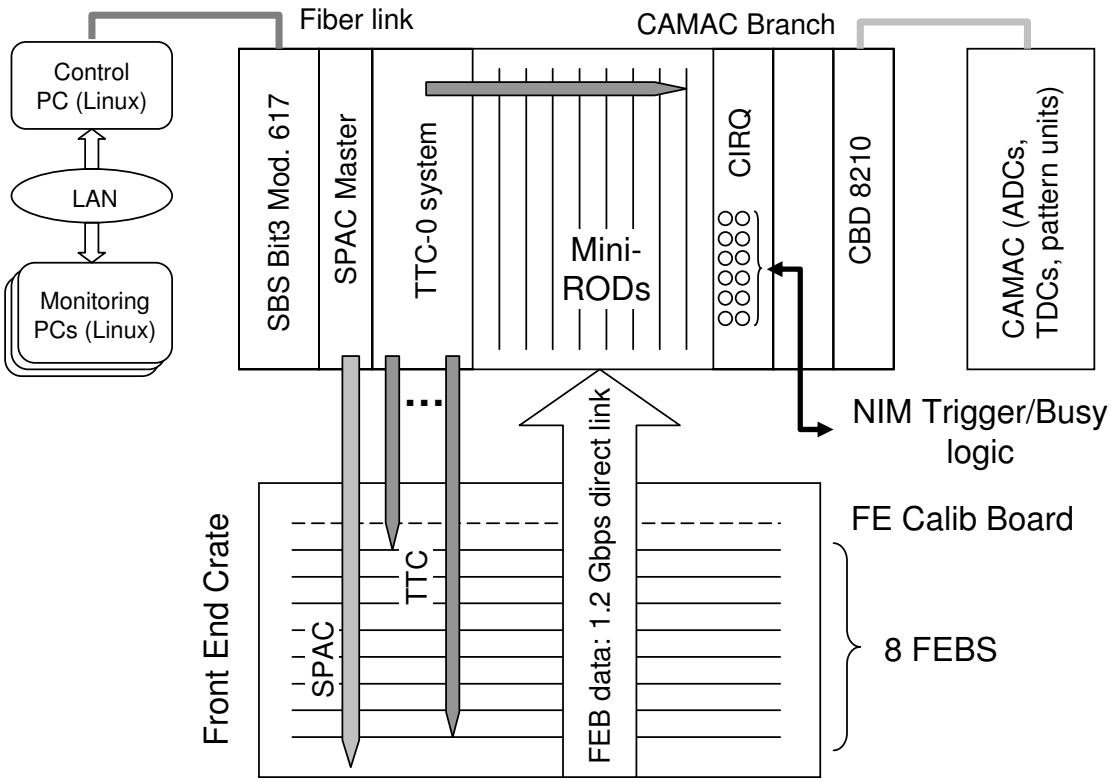

Figure 9. Schematic of the beam test readout and data-acquisition setup.

boards to the baseplane of the Front End Crate via a cryogenic signal feedthrough. High voltage was applied through a separate feedthrough as will also be the case in ATLAS. On the FEBs, the signal for each channel is amplified and shaped with a bipolar shaper, then sampled every 25 ns, in time with the Trigger Timing Control (TTC) clock. Samples are stored in a switched capacitor array (SCA) analog pipeline, to be digitized and read out in the event of a trigger. Each readout channel has three possible gains. Configuration of the FEBs can specify which gains are read out, as well as the number of samples to be digitized and recorded. For most of the data taking the system was run in "auto-gain" mode, which makes use of predefined thresholds for switching between gains (between High and Medium gain in the case of this beam test). Readout of the samples from the FEBs was done using miniRODs (where ROD stands for Readout Driver) which were designed for the FEB readout in previous ATLAS LAr Calorimeter beam tests [9, 10].

The readout system is illustrated in figure 9. The data acquisition system was built around a single control VME crate located at the cryostat platform, near the Front End Crate and the trigger logic NIM crates. It contained:

- eight miniRODs, directly connected to the eight FEBs by 1.2 Gbps data links;
- the TTC-0 system to synchronize the FEBs and miniRODs (TTC-0 is the prototype TTC system, inherited from previous LAr calorimeter beam tests [9, 10], together with the miniRODs);

2008 JINST 3 P02002

- the SPAC-master unit for the SPAC bus [11], which is used to configure and control the FEBs and the calibration board;
- a 6-channel trigger input/busy unit (CIRQ [12]) serving as the interface to the trigger NIM logic;
- the CAMAC interface board (CES CBD 8210), to drive a CAMAC crate with TDCs, ADCs and pattern units;
- an SBS-Bit3 Model 617 PCI to VME bus adapter, with a 50 m fiber link to the control PC.

The system was controlled by a remote Linux PC running a dedicated run control application with an inter-process communication scheme based on the ControlHost technology [13]. The FEB, TTC and SPAC interface libraries were adopted from a previous LAr beam test DAQ [10]. The FEB event data was buffered autonomously by the miniRODs. The VME-PCI fiber link provided a direct access to this data which was formatted by the readout application running on the control PC and stored, asynchronously, on a 1.2 TB RAID system. The operation during the run was driven by the triggers registered by the CIRQ module. The read-out speed was sufficient to avoid the need for buffering, i.e. every event (up to several hundred events per spill) was transferred immediately after the completion of the FEB readout. Several online monitoring processes could be run concurrently with the data taking, on remote PCs connected to the local network. For example, the online beam profile measurement from the BPCs was particularly useful for beam tuning. Because of its compactness, the FCal DAQ system was manageable and provided a robust operation during the extended data-taking period.

Since beam triggers arrive asynchronously with respect to the TTC clock, it was also necessary, for each event, to measure the time delay between the TTC clock and trigger. This was digitized with 50 *ps* resolution using the beam counter S1 and the TTC 40MHz clock pulses as Start and Stop signals for the LeCroy 2228A TDC. Since the relative phase of TTC sequence and the beam trigger is random, measurement uncertainty occurs when the trigger and TTC pulses coincide and the phase jumps from 0 to 2π. To remove this ambiguity, a second TDC input was stopped by a TTC pulse sequence delayed by about 10 ns, i.e. roughly half a period.

The front-end crate additionally contained a prototype pulser board that delivered calibration pulses directly to the front-end electronics via a special board mounted to the backplane of the Front End Crate. This pulser system was used for a variety of calibration runs that will be briefly described in the next section. For the analysis presented here these data were mainly used for determining channel-by-channel gain variations which were about 2% rms. These corrections were normalized to provide an average of 1.00 over the 994 instrumented channels.

3. Data taking, data handling

Data were taken over two extended periods in the summer and fall of 2003, using the H6 beamline at CERN. This beamline can provide electron, hadron and muons beams at energies up to about 200 GeV. Electron and hadron data were taken at each of the five impact points described earlier. For the energy scan, data were taken at the 4L and 4H positions with beam energies spanning the energy range from 10-200 GeV. Some 200 GeV muon data were also taken. For the scan of the

2008 JINST 3 P02002

Table 1. Statistics (in thousands of triggers) recorded for good electron and hadron runs at the two impact points used for the energy calibration. Actual energies for the 150 and 200 GeV electron beams are 147.8 GeV and 193.1 GeV, respectively.

Beam	Nominal Beam Energy (GeV)								
type	10	20	40	60	80	100	120	150	200
e 4L	396	504	216	204	216	216		204	432
e 4H	192	192	300	252	228	216		204	228
π 4L	1086		900	408	816	414	612	612	672
π 4H	960	408	780	816	660	444	612	629	648

inner edge of the FCal, only the highest energy electron and hadron beams were used. As stated earlier, analysis of the 4H and position scan data will be described in future publications.

While electrons are required to set the electromagnetic scale of the FCal1, the forward calorimeter is primarily intended to extend calorimetric hermeticity for jets to the high $|\eta|$ region. For this reason, and because of the poorer resolution for hadronic energy reconstruction, more time was dedicated to hadron running than to electrons. The desired goal was at least 200K electron triggers at each energy and impact point, and at least 400K hadron triggers. These statistics were achieved and in most cases exceeded, with a couple of exceptions: at 120 GeV we were unable to obtain a sufficiently clean electron beam, while at 20 GeV the hadron beam quality was poor and insufficient statistics were accumulated at the 4L position.

Good runs are those corresponding to good beam conditions, proper setup of any material placed into the iron wall to model upstream material, and proper functioning of all beamline elements and readout electronics. For two series of early runs, some coherent noise was introduced by using the calibration board to inject monitor pulses in between beam spills, a procedure which was stopped after the problem was identified. Under normal running conditions, coherent noise on the FEBs, on average, represents about 10% of the noise per channel. As described later on, the analysis of the data accounts for noise contributions run by run; these data are therefore included in the analysis. For the energy scans, after selecting good runs we are left with the statistics summarized in table 1. Not shown are the statistics for the position scan points, where only the highest energy beams were used; at each of these points about 200K electron and 600K hadron triggers were recorded.

Standard data-taking was in auto-gain mode with 7 samples. For special data and for some calibration runs the number of samples taken was increased (to 16, 24, or 32). In order to limit data files to sizes not exceeding the capacity of a standard CD-RW disk, data was taken in runs corresponding to 12,000 beam triggers (in the case of 7 sample running). The data for each run also contains approximately 5% of random beam triggers.

In addition to the particle beam data, a large amount of calibration data was accumulated. Dedicated pedestal runs were taken at regular intervals, as were different types of runs utilizing the FCal calibration pulser board, to allow study of the electronics gain, channel-by-channel gain variations, cross-talk, and response non-linearities. These run types differed in the pattern of pulsed channels, the pulse amplitude (DAC value) and the delay of the applied signals with respect to the

2008 JINST 3 P02002

TTC clock, as described below:

- **Standard calibration runs:** these runs performed a fine scan of DAC values from 0 to the maximum of 16000, using a fixed delay with the peak near the fourth sample. Seven samples were recorded for each gain, and all channels were pulsed in each event.
- **Long calibration runs:** these runs performed a coarse delay scan (0-21ns in steps of 3ns) with 12 DAC values in the range 0-4000 chosen so there were no overflows in medium gain; 24 samples were recorded for 2 gain settings (High, Medium), with 1 channel/event pulsed.
- **Cross-talk and auto-gain runs:** these were similar to the long calibration runs but had automatic gain selection and fewer (1 or 3) DAC settings. The same 8 delays settings as in the long calibration runs were used and 24 samples were recorded.

3.1 Treatment of data

Previous ATLAS LAr calorimeter beam tests at CERN have relied on dedicated software packages developed specifically for the data analysis, and much past effort has been put both into maintaining these software packages and later into converting them to Athena, the ATLAS software framework. For this beam test, the decision was taken early on to use Athena both for the (quasi-online) monitoring during the data taking, and for reconstruction and analysis of data. The analysis presented in this paper was performed with Athena version 11.0.41, except for analysis of the data taken with the calibration pulser, which was performed using stand-alone code. A more detailed description of the treatment of beamline and calorimeter data is given in the next two sections.

3.2 Treatment of data from beam line elements

In the offline selection of events for analysis, in addition to the beam trigger, requirements were placed on additional bits in the trigger word. Events were rejected if any one of the EarlyPU, LatePU, or Veto trigger bits was set. Information from the CEDAR was also used in both the electron and pion selections, as described further on.

A more sophisticated "beam cleaning" procedure, based on analog information from the various beam instruments, has also been used to reduce contributions from beam particles that have scattered upstream of the calorimeter or events in which there are multiple beam particles. Pedestal values for all counters were determined on a run-by-run basis, including corrections for pedestal drift within each run. For each beam element, the single-particle response was then determined by fitting the observed spectrum. Based on the pedestal width and the single-particle spectrum parameters, a set of software thresholds was defined for each counter. This allows suppression of a variety of undesired events. As an example, the signals from S1, S2, and S3 were required to exceed the set thresholds, in order to remove events in which the beam particle hit the light guide or grazed the edge of the counters.

Hit information from the BPCs is used to fit straight tracks, separately in the *xz* and *yz* planes. The χ^2 values from these fits are taken as a measure of the fit quality, to exclude, for instance, tracks that scatter in the beamline materials. The fit results also yield information on the relationship between the position of a beam particle within the beam spot, and the slope of it's trajectory. These two pieces of information can be combined to define a "Beam Envelope" which differs for

2008 JINST 3 P02002

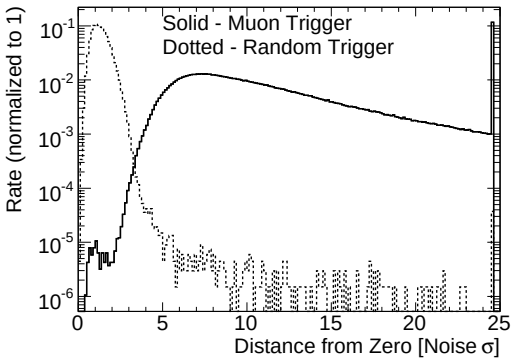

Figure 10. The muon energy spectrum in the tail catcher and the associated pedestal (noise) distribution.

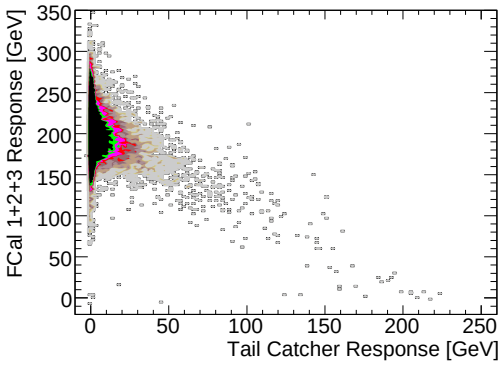

Figure 11. Reconstructed FCal energy at the EM scale plotted against the energy in the Tail-catcher.

the electron and hadron components of the beam and so allows for separation of electrons and hadrons. Similar beam cleaning and beam envelope techniques have been used in analyses of previous Forward Calorimeter beam test data [6, 14].

Muon contamination in the electron beams is suppressed by requiring that the Muon counter response be below 2σ of the noise. For muon studies used for calibration of the tail-catcher, to be discussed below, there was an additional requirement that the signal be consistent with that of a single MIP. Since the coverage of the Muon counter is limited, additional suppression of muons is obtained using information from the tail-catcher.

3.3 Treatment of tail-catcher data

The analog data from the tail-catcher was pre-processed in a way similar to that described above for the beam counters. In this case, the two outputs from each plane required determination of the gain ratios, which was extracted from an analysis of all events with visible longitudinal leakage. In contrast to the studies performed for the beam counters, the available muon statistics did not permit run-by-run MIP response parameter determination. Instead, blocks of consecutive runs taken under the same conditions were used.

The tail-catcher performance for muon detection is shown in figure 10. The tail-catcher calibration for the conversion from MIPs to GeV of hadronic energy was obtained from an analysis of the 200 GeV hadron samples (which has the maximum leakage); this calibration constant is close to 8 MIP/GeV. The correlation between the FCal Signal (at the EM scale) and the tail-catcher response, is shown in figure 11. In the analysis presented here, the tail-catcher was used only in a veto mode, to reduce muon and hadron contamination in the electron runs. It may be more fully used in future analyses of the hadronic data, to assist in the development of a leakage correction routine based solely on FCal information.

3.4 Treatment of calorimeter data

As described earlier, the readout of the calorimeter system was configurable, allowing for different numbers of samples and different choices of gain. Seven samples per channel per event were normally used for both data and calibration runs. The first sample was used for pedestal and noise

2008 JINST 3 P02002

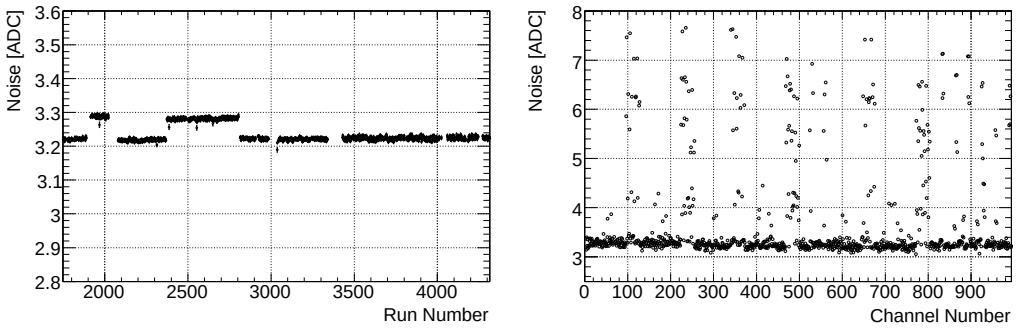

Figure 12. The plot on the left shows the average noise, in ADC counts, vs. run number, over the full range of good runs. On the right, the average noise is shown vs. channel number for data taken during one of the noisy periods visible in the left-hand plot.

studies and samples 2 through 6 were used to calculate the pulse amplitude for physics studies. The readout was usually configured in auto-gain mode, in which the gain switched automatically between high and medium gain, at a specified threshold. At the available beam energies, signals were mostly recorded at high gain. Low gain was not used.

Pedestal and noise values were calculated for each channel run-by-run and stored in a database. The pedestal value for a channel was taken as the average value of the first readout sample over a given run. These pedestals were derived from the physics run data and so exist only for the high gain readout. In the case of channels read out using medium gain, pedestals were derived from a single, dedicated dual-gain pedestal run. Medium gain pedestals are needed primarily for the analysis of the high energy electron data, which was all accumulated during a two-week period. A number of these dual-gain pedestal runs were taken throughout this period and show the pedestals to be stable over that time period.

The noise for each channel was calculated as the standard deviation of the pedestal value for each run. The mean value of the noise for all channels as a function of run number is shown in figure 12. The average value of about 3.2 ADC counts is consistent with expectations. This figure clearly shows that there were blocks of runs early in the beam test that had higher noise. The problem was understood and corrected after the second block of affected runs. Data from the noisy runs is shown in the right-hand plot of figure 12, as a function of the channel number, illustrating that the higher noise was associated with particular channels. Data from the two noisy periods was used in the analysis, but, as will be described later on, noise contributions are accounted for channel-by-channel and run-by-run and subtracted in quadrature in the resolution studies.

Pulse height and timing information were extracted from the sampled data using the Optimal Filtering (OF) technique [15]. This is the standard procedure in use by the ATLAS Liquid Argon Calorimeter group. It uses a simple but fast algebraic expression to calculate the peak amplitude and peak time from the pedestal-subtracted, time-ordered samples. The calculation requires a set of Optimal Filtering Coefficients (OFCs); derivation of these in turn requires a precise representation of the pulse shape and knowledge of the noise autocorrelation matrix, both of which can be obtained from the beam test data.

The signal out of the shaper is sampled every 25 ns, in synch with the TTC clock. Since the

2008 JINST 3 P02002

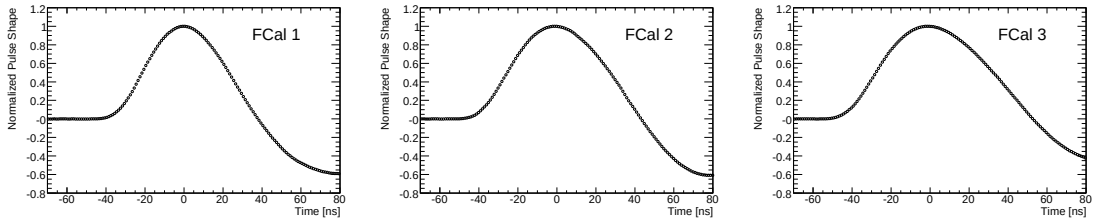

Figure 13. Reference pulse shapes for FCal1, FCal2 and FCal3, obtained from the beam test data and used for calculation of the OFCs used for the signal reconstruction.

phase of this clock is random relative to the beam triggers, the calorimeter pulses come at random times relative to this clock. The timing was adjusted so that, on average, the peak of the pulse falls at the 4th (out of seven) samples. However, pulses can be as much as 12.5 ns ahead or behind this average case.

The pulse shapes used for input to the OFC calculation were reconstructed from the data, by starting with a pulse shape prediction from a SPICE model of the electronics chain and performing an iterative fit procedure. Noise contributions were accounted for by using the noise autocorrelation matrix, the inverse of which forms the weight matrix in the χ^2 sum to be minimized. The pulse shape prediction was fitted to the pedestal-subtracted samples from a large number of events to determine the peak height and time for each event, using only events with a sufficiently large peak. Then, for each of these events, the samples were shifted in time so that the peak time was at the time origin. The pedestal-subtracted sample amplitudes were scaled to yield a peak of unit height. Plotting the samples from all of the events, so obtained, yielded a pulse shape that appeared as a fuzzy curve, the smearing being due to the very small electronics noise. The small difference between the mean of this fuzzy line and the SPICE model pulse shape was parameterized by a polynomial. Adding the polynomial to the SPICE pulse yielded an improved pulse shape which was input to a second iteration, after which the pulse shape was stable. Pulse shapes differ from module to module due to the different drift times associated with the different LAr gap sizes, but the pulse shape for a given FCal module is rather uniform from channel to channel and use of a single pulse shape per module yields an adequate calibration. The pulse shapes obtained from the beam test data and used for calculation of the OFCs are shown for each module in figure 13.

In ATLAS, the amplitude and timing of a signal pulse are determined by application of the appropriate set of OFCs, one set for the energy reconstruction and another for the timing. During normal ATLAS data-taking with p-p collisions, the TTC clock that sets the sampling times will be in phase with the LHC bunch crossing clock. This means the signal from a given channel will always be in the same phase with respect to the TTC clock; consequently only one set of OFCs per channel will be required. This is not the case for the beam test in which the beam particles arrive asynchronously with respect to the TTC clock. To use the OF technique in this case, it is necessary to measure the phase between the beam trigger and the readout clock and select the corresponding set of OFCs, which were generated in bins of 1 ns. This is adequate for good energy reconstruction, as illustrated in figure 14, which shows the effect, on the reconstructed energy and time, of introducing an artificial time shift between the data and the set of applied OFCs. For shifts of less than 2 ns there is essentially no effect on the reconstructed peak amplitude.

2008 JINST 3 P02002

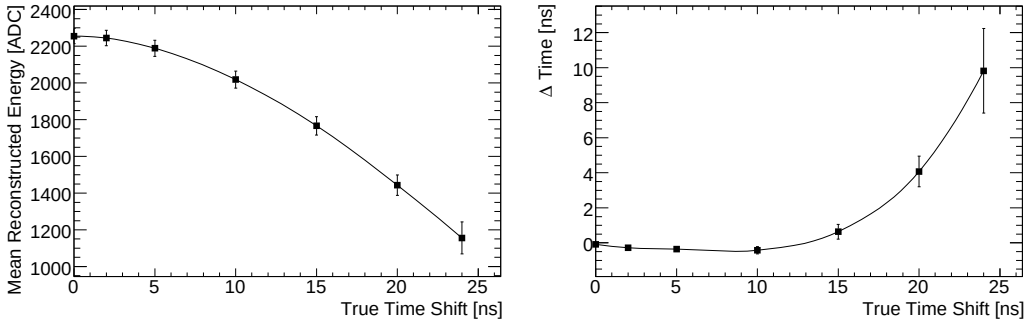

Figure 14. Reconstructed peak amplitude and time using OFCs with an artificial time shift.

4. Data analysis

This paper focuses on the analysis of the beam test data taken at the 4L beam position. In this case, there was a minimal amount of material in front of the calorimeter and the impact position on the calorimeter face provides for approximate containment. Using these data we evaluate the intrinsic performance of the ATLAS forward calorimeter, for electrons and hadrons.

4.1 Signal reconstruction

The amplitude (in ADC counts) and the timing for each channel were reconstructed using the OFC technique as described in section 3.4. For both electrons and pions a cylindrical clustering technique was used, in which the reconstructed energy was obtained by summing the energies of all channels within a certain radial distance of the beam impact point. The impact point was obtained from extrapolation of beam particle tracks, reconstructed from the BPC data; distances were calculated based on the center of each readout channel. For electromagnetic showers, about 99% of the energy is deposited within an 8 cm cylinder centred on the electron impact point. For pions, a larger cut is required for containment of the broader hadronic showers. As will be described below, contributions from any residual hadron contamination in the electron data are modeled using the hadron data taken at the same energy. In this case, the hadron data was analyzed with the same cylinder radius as is used for the electrons. All channels affected by high-voltage shorts were sufficiently far from the 4L positions that they do not affect the results reported here.

In order to determine the beam impact point on the calorimeter, the coordinate system defined by the tracking chambers must be mapped onto that of the calorimeter. The first step in this procedure is to map the impact point obtained by extrapolation of the electron tracks, onto the centre-of-gravity of electromagnetic clusters in the FCal1. However, it is observed that these centres-of-gravity are pulled towards the geometric cell centres, so fine-tuning is performed by looking at energy sharing between neighboring cells. Scans across cell boundaries were done in x and y and the ratio $E_{1,max}/E_1$ was evaluated as a function of position, where $E_{1,max}$ is the energy in the channel with the highest energy and E_1 is the total energy in the FCal1. The minimum of this distribution is then associated with the average of the positions (in x or y, respectively) of the electrodes along the edges of the two cells. These distributions are shown in figure 15, which have already been corrected for the measured shifts. The distribution in x (horizontal direction in fig-

2008 JINST 3 P02002

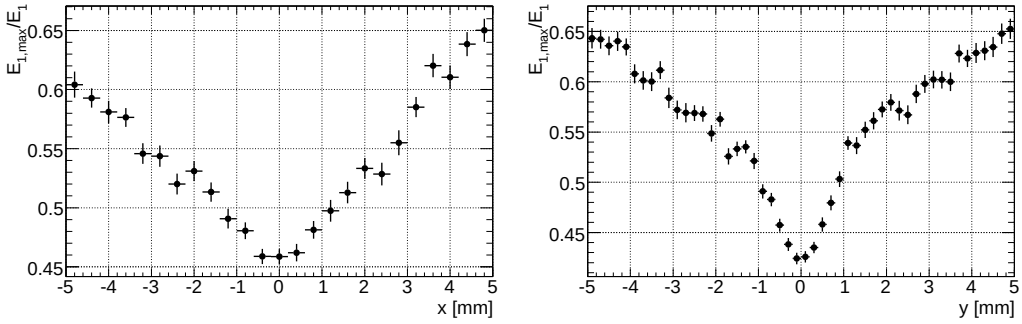

Figure 15. Plots of $E_{1,max}/E_1$, vs. the corrected x and y position of the beam track extrapolated to the front face of the FCal1. The quantities $E_{1,max}$ and E_1 are as defined in the text.

ure 3) is broader due to the cell boundary in x being irregular, while the boundary in y is straight. The slight asymmetry in $\pm x$ is due to the the $\sim 3^\circ$ impact angle, which is in the horizontal plane of the module and thus has the beam pointing slighty towards positive values of x.

Noise contributions to the signal are accounted for in the following way: noise files are created run by run, containing the reconstructed noise for each channel, obtained from the analysis of random-trigger events. For each cell, in each random triggered event, the reconstructed energy is obtained by selecting a random phase and reconstructing the signal using the corresponding set of OFCs. All random events in the run were processed in this way to produce a noise file that associates an average reconstructed noise with each readout channel in each run. In the reconstruction of physics events, each cluster corresponds to a well defined set of readout channels; the noise level associated with a particular cluster can be obtained by sampling from the noise file for that run, for each channel associated with the reconstructed cluster. This procedure allows for an accounting of run-by-run variations in noise levels and extends well to more sophisticated clustering algorithms, for instance the topological clustering algorithm that is one of the proposed methods for ATLAS.

4.2 Analysis of electron data

Beam particles were selected as described in section 3, including the beam cleaning and beam envelope cuts, and the use of the tail-catcher for suppression of muons and residual hadron contamination. The CEDAR was used only for the 60 GeV sample where the hadron contamination was particularly large. This results in relatively poor statistics for this point. For accepted events, the energy reconstruction in each of the FCal modules was performed as described above. The results presented below, for the response to electrons, were obtained using 8 cm cylinder clustering for the FCal1 only.

Even after the beam cleaning and beam envelope cuts, the electron samples are not pure, so proper extraction of the performance for electrons requires some method for dealing with the residual hadron contamination, since the high-energy tail of this contribution falls beneath the electron peak. After application of the beam cleaning and beam envelope cuts, any residual hadron contamination is accounted for by using the hadron data, taken at the same energy and impact position, to model that contribution to the reconstructed electron energy distribution. As an example, the reconstructed energy distribution obtained from the 150 GeV electron sample at the 4L position is

2008 JINST 3 P02002

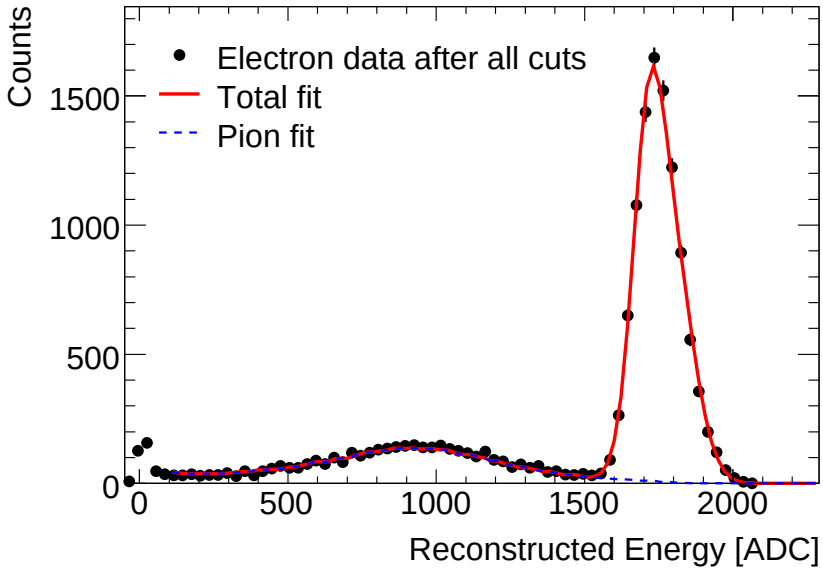

Figure 16. Reconstructed energy for the 150 GeV electron beam at the 4L position using cylindrical clustering in the FCal1. Energies are presented in ADC counts at the high-gain scale. Overlaid is the result of the fit described in the text, which takes the shape of the hadron distribution from the hadron data taken at the same energy and impact position.

shown in figure 16, where one clearly sees a large peak from the electrons and an intermediate (and broader) peak from hadrons. The expected signal shape is slightly non-Gaussian due to the impact point variation of the FCal response [6]. This effect is most pronounced at the higher energies. The reconstructed energy spectrum is fitted with a function consisting of the sum of a double Gaussian, parameterizing the signal, and a description of the hadron contribution with a shape obtained from analysis of the hadron data (taken at the same energy and position) and a normalization that is allowed to float. As a systematic study, the double-Gaussian fit was performed in two different ways. In the first, all six parameters were allowed to vary in the fit. In the second, at all energies, the ratio of the means of the two Gaussians and the relative populations were constrained to have the values obtained from the fit to the 200 GeV data. The latter constraint is motivated by the hypothesis that the relative population of the two Gaussians is dominantly determined by the geometry of the unit cell, i.e. the relative populations of different beam-particle impact points with respect to the centre of the closest electrode. These two fit procedures yield almost identical results. A single Gaussian parameterization was also examined. This provides a much poorer fit in the signal region, but the extracted signal parameters are not dramatically affected. Each fit was done over the full range of reconstructed energies, excluding the region near zero where muons can contribute. The reconstructed energy and resolution are determined from the parameters of the two Gaussians fitted to the signal peak. This fit technique requires that we have the corresponding hadron data with which to model hadron contamination. This is not the case for the 20 GeV sample. The results of the analysis of the electron data at each of the beam energies are shown in figure 17, with the results of the fits (as defined in figure 16) overlaid. In the case of the 20 GeV data the fit function was a double Gaussian only, since no hadron data was available. Results are presented on a logarithmic vertical

2008 JINST 3 P02002

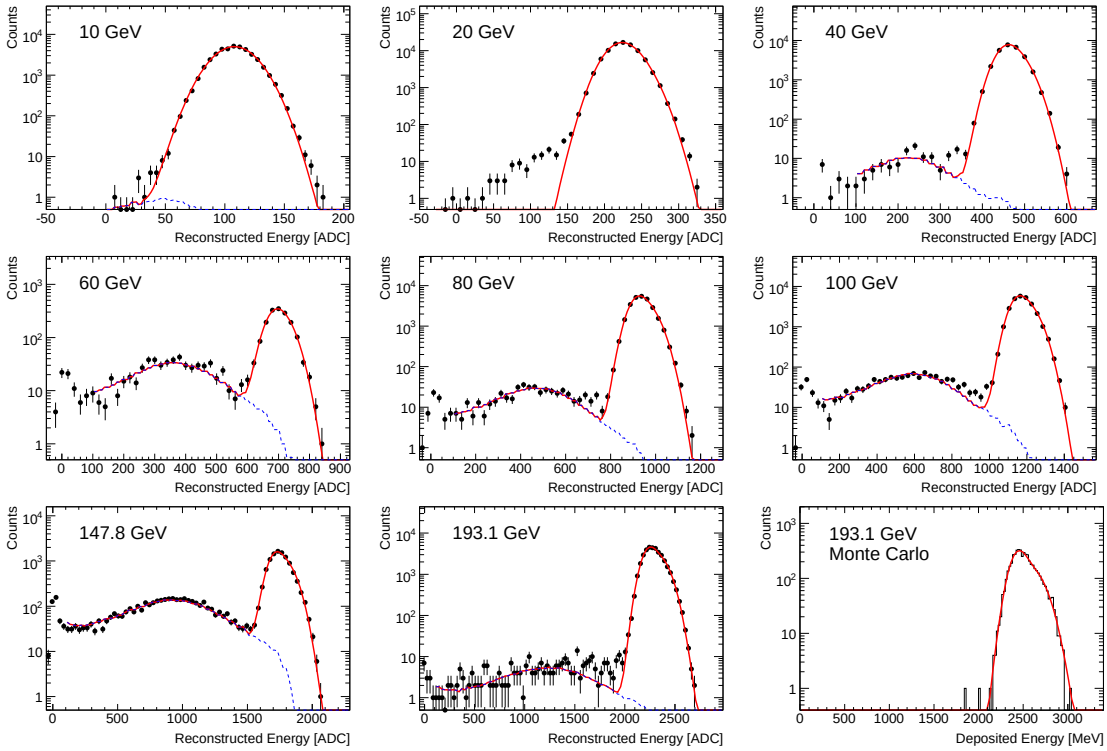

Figure 17. Energy spectra from electron data at 4L, obtained using an 8 cm cylinder sum. In each case the points represent the data and the overlaid fit results are as defined for figure 16 and described in the text. Also shown (bottom right) is the distribution of deposited energy, in the FCal1 liquid argon gaps, from a Monte Carlo simulation of the beam test setup and detector, for 193.1 GeV electrons.

scale in order to illustrate the tails of the distribution. Also shown is the distribution of energy deposited in the FCal1 liquid argon gaps, by 193.1 GeV electrons, from a Monte Carlo simulation of the detector and beamline. Overlaid is the result of the double-Gaussian fit, demonstrating that this parameterization provides a good description of the signal shape.

An important aspect of past and current beam test studies is the extraction of the electromagnetic scales of the FCal modules, since this also forms the starting point for hadronic calibration. In a previous beam test [6], which utilized prototype modules and different readout electronics, both the FCal1 and FCal2 were exposed to electron beams to allow determination of the relative electromagnetic scale factors. In 2003 only the FCal1 module was directly exposed to electron beams. Based on the results of the fits displayed in figure 17, the FCal1 response to electrons (in ADC counts at the high gain scale) is shown as a function of beam energy in figure 18. Also shown are the residuals relative to the results of a linear fit, the result of which is overlaid. The response is linear to within about $\pm 0.5\%$ over the energy range from 10-200 GeV. The higher energy electrons were from a secondary beam, the polarity of which is determined by the beam definition in the neighbouring H8 beamline. However, the lower energy electrons were taken with a tertiary beam for which one can select the polarity. At the lowest energies, ($E \leq 20$ GeV), data was taken for both electrons and positrons to allow for systematic checks. Small differences in the mean response to

2008 JINST 3 P02002

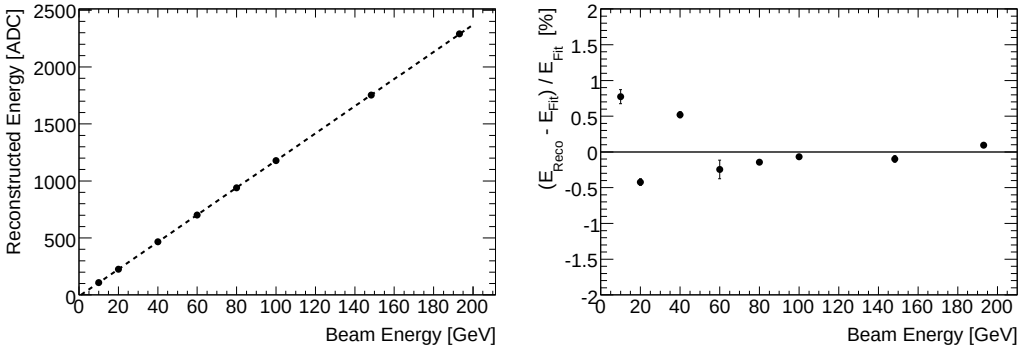

Figure 18. Linearity of the FCal response to electron and the residuals with respect to the linear fit. The errors shown are statistical only. The systematic uncertainties are discussed in the text.

electron and positrons at these energies were observed and lead us to assign systematic uncertainties on the reconstructed energy of 0.9% at 10 GeV and 0.6% at 20 GeV. These values are consistent with the size of the observed deviations from linearity in this energy range. At all other energies, only single polarity data was taken: electrons at 60, 150 and 200 GeV, and positrons at 40, 80 and 100 GeV, so it is not known whether a similar systematic uncertainty applies to the measurements at these energies. Magnets were not systematically degaussed during the beam test, so there may be small contributions to the beam energy uncertainties due to remnant fields. However such an effect would be expected to be in the same direction for all of the low energy points, since they were taken during the same period with no intervening beam manipulations that would account for a sign change. Other systematic uncertainties arise due to event selection, fitting procedures, and to residual effects associated with the combination of the response dependence on the beam particle impact point and variation in the beam profiles at each energy. The total uncertainty from these sources is estimated to be about (0.1 - 0.2) %. The possible existence of an unidentified systematic uncertainty at the 0.5% level (in the low energy region) cannot be discounted. The fitted slope corresponds to an electromagnetic scale factor of $12.07 \pm 0.07(stat) \pm 0.07(syst)$ ADC counts / GeV. Allowing for increased uncertainties in the reconstructed energies, large enough to account for the observed deviations from linearity, makes only a small contribution to the systematic uncertainty. The average gain correction for channels contributing to the electron energy reconstruction was examined and found to be 0.988. This factor is accounted for in the analysis.

In advance of the calibration beam test, predictions were made of the energy calibration constants, for each of the three modules. A feature of liquid argon sampling calorimetry is that the common parameters which determine the energy response are already known. Differences between one liquid argon calorimeter and another are mostly due to geometry. Since the geometry of the forward calorimeter modules is well known, calculations of the response should be reliable. The predictions utilize knowledge of the cold and warm electronics which could also be calculated from first principles, and measurements were available to confirm the calculations. The initial calculation of the FCal1 energy calibration agreed with the experimentally determined value at the 5% level. However, using the extensive calibration data taken during the beam test, some small impedance mismatches were identified, which were not accounted for in the initial predic-

2008 JINST 3 P02002

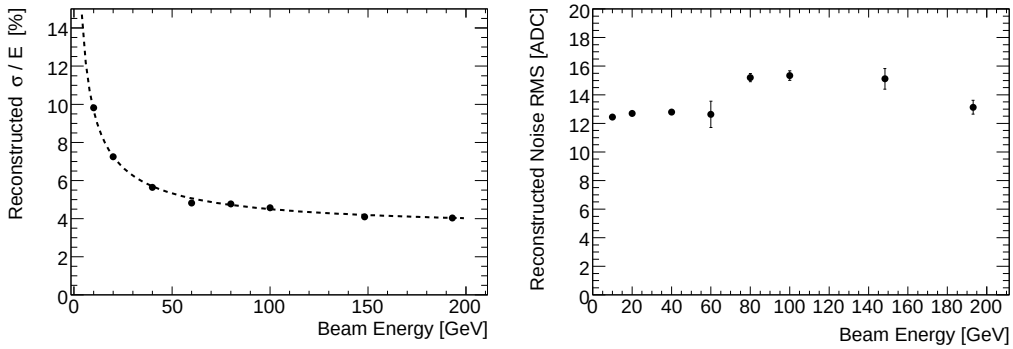

Figure 19. Left hand plot: Electron resolution for electron data showing a sampling term of 28.5% and a constant term of 3.5%. The right-hand plot shows the noise subtracted (in ADC counts at the high-gain scale) at each energy point.

2008 JINST 3 P02002

tion. Including these effects in the modeling of the electronics leads to a predicted scale factor of 12.0 ADC / GeV, in good agreement with the experimental result. This agreement is important in light of the fact that final ATLAS readout electronics were unavailable for the 2003 beam test, so carrying the calibration derived from this beam test over to ATLAS will rely on simulations of the old and new electronics chains. For the hadronic modules, the simulation predicts the corresponding scale factors to be 6.1 ADC/GeV for the FCal2 and 5.4 ADC/GeV for the FCal3. The ratio of the FCal1 and FCal2 responses has been measured in a previous beam test [6] and is consistent with the ratio of these calculated values at the 5% level. These three scale factors are used in the hadronic energy reconstruction discussed later on. The linearity fit yields an intercept of -12.3 ADC counts, corresponding to an energy of about 1 GeV, which might be attributed to energy losses upstream of the calorimeter. Attempts were made to model this energy loss in a simulation of the beamline. This yielded predicted energy losses which varied from about 450 MeV at 10 GeV, up to 1.1 GeV at 200 GeV. However, the simulation accounted only for material located downstream of the final bend magnet, not for material further upstream, such as the high-pressure gas volume in the CEDAR, or regions where the H6 beam passed through a significant thickness of air. For this reason, no attempt has been made to correct for the upstream energy loss and the intercept was allowed to vary freely in the linearity fit.

The noise-subtracted energy resolution as a function of energy is shown in figure 19 along with the result of a fit using the function:

$$\frac{\sigma_E}{E} = \frac{a}{\sqrt{E}} \oplus b. \tag{4.1}$$

The right-hand plot shows the subtracted noise (in ADC counts, at high gain) at each energy point, obtained as described earlier. The fit results are $a = (28.5 \pm 1.0)\% \cdot GeV^{1/2}$ and $b = (3.5 \pm 0.1)$ %. The constant term is consistent with that obtained in a previous beam test while the stochastic term is somewhat improved over the previous result [6]. The statistical uncertainties are small; the quoted uncertainties are dominated by systematics associated with the choice of selection criteria, cylinder cluster radius, and fitting procedures.

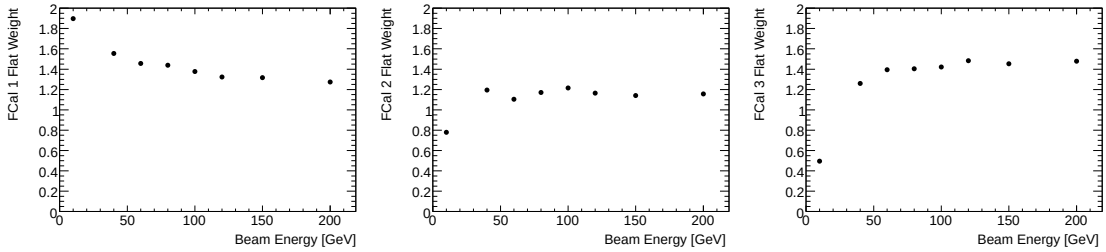

Figure 20. The flat weights for hadronic reconstruction, for each FCal module, as a function of energy.

4.3 Analysis of hadron data

Energy reconstruction for the hadron data involves the combination of the energy deposited in three individual FCal modules, each of which has a different sampling fraction and thus a different electromagnetic scale. Each module additionally has a different relative response to electrons and hadrons. Both effects must be accounted for when combining information from the three modules for the reconstruction of total hadronic energy. This was done using a "flat-weighting" technique in which the energy is reconstructed from cells within a 16 cm radius of the beam-particle impact point, as a sum of the form

$$E = g_1\alpha_1(ADC_{\mathrm{FCal1}}) + g_2\alpha_2(ADC_{\mathrm{FCal2}}) + g_3\alpha_3(ADC_{\mathrm{FCal3}}) \tag{4.2}$$

where α_1, α_2 and α_3 are the ADC→GeV electromagnetic scale factors for the three modules and g_1, g_2 and g_3 are chosen to minimize the energy resolution, with the constraint that the average reconstructed energy equal the known beam energy. Initial data analysis showed slightly different responses to hadron beams of different polarities. This was attributed to a significant level of proton contamination in the positive beams (10, 20, 40 and 80 GeV). For this reason, a CEDAR requirement was included in the pion selection criteria. This requirement was applied at all energies, regardless of the beam polarity, except at 200 GeV, as the CEDAR was not functioning when those data were recorded. However, for the negative polarity beams, the effect on the reconstructed energy and resolution was very small.

The flat weights were derived separately at each energy and are shown for each module, as a function of energy, in figure 20. Since energy-dependent weights cannot be used at ATLAS, a single set of weights is used for the reconstruction at all energies. In ATLAS, most of the jets in the forward calorimeter will be very high energy, so the highest energy weights are considered the most applicable; the results presented below were therefore obtained using the weights derived from the highest energy (200 GeV) data sample. The spread of the weights from the four highest energy points is used in the evaluation of the systematic uncertainties. Because the structure of the two hadronic modules is very similar, one would expect that the weights for the two modules would be similar. This is the case if one accounts for the energy in the tail-catcher when extracting the weights. However, since the tailcatcher will not be present in ATLAS the weights are calculated without accounting for longitudinal leakage, which leads to an increase in the weights for the FCal3.

2008 JINST 3 P02002

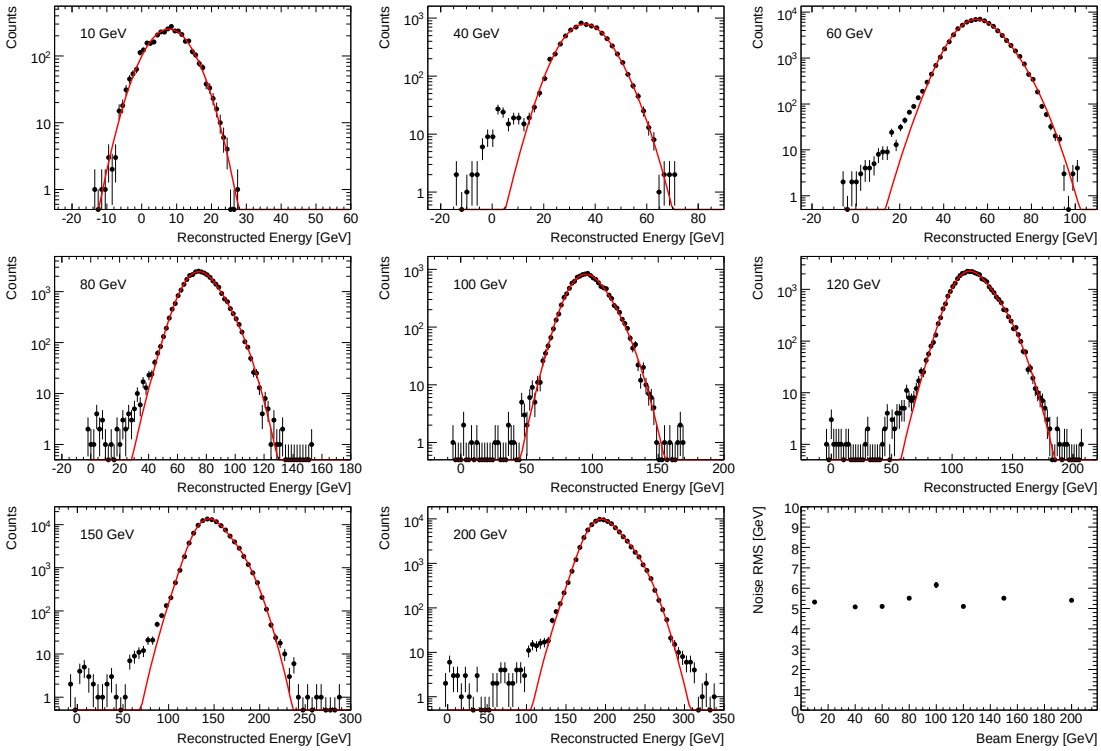

Figure 21. Distributions of reconstructed energy for pion data taken at the 4L position, reconstructed using the flat-weighting technique. Also shown is a plot of the reconstructed noise at each channel, obtained in the manner described in the text.

Figure 21 shows the distributions of reconstructed energy at each beam energy, for pions selected from the hadronic data taken at the 4L position, using the flat weights extracted from the 200 GeV data. Also shown is the average reconstructed noise at each beam energy. From these distributions we derive the FCal energy response and resolution function for pions. Several methods have been used; the mean and width of the distributions have been taken directly from the observed distributions as well as from fits using single- and double-Gaussian parameterizations. For the double-Gaussian description, both the four and six parameter fits were performed, as in the analysis of the electron data described in section 4.2. The four parameter double-Gaussian fit results are used to extract the response and resolution results shown below, while the other methods are used in the evaluation of systematic uncertainties. The plots are again presented on a logarithmic scale to illustrate the extent of the tails, which is an important performance criterion, as discussed later on.

In figure 22, the plot on the left shows the ratio of the reconstructed energy to the beam energy, as a function of the latter. The right-hand plot shows the noise-subtracted energy resolution for pions, as a function of the beam energy. Overlaid is the result of fit to the resolution parameterization described earlier. The stochastic and constant terms are $(94.2 \pm 1.6)\% \cdot \mathrm{GeV}^{1/2}$ and $(7.5 \pm 0.4)\%$ respectively, which meet ATLAS requirements. Uncertainties are again dominated by systematics, which are taken as the full range of variation seen with use of the four sets of weights and from variation of the selection criteria and fitting procedures.

2008 JINST 3 P02002

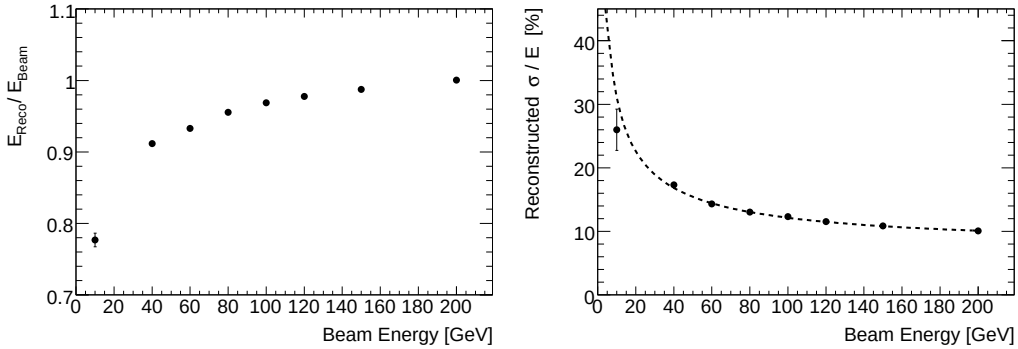

Figure 22. For pions, the plot on the left shows the ratio of the reconstructed energy to the beam energy, as a function of the beam energy. The plot on the right shows the noise-subtracted energy resolution as a function of beam energy. Overlaid is the result of the fit described in the text.

4.4 Hadronic reconstruction with radial weights

More sophisticated weighting schemes are often used to improve hadronic resolution. Here we illustrate one such procedure, a radial weighting technique [16] which exploits the fine transverse segmentation of the FCal modules. In this case, for each event, the energy is reconstructed as the sum:

$$E = \sum_{j=1}^{\text{ncells}} S_j \times W_k(R_j). \tag{4.3}$$

Here S_j is the energy of the j^{th} cell, reconstructed at the appropriate electromagnetic scale, $W_k(R_j)$ is a radial weight factor, and R_j is the distance between the j^{th} cell and the particle impact point on the calorimeter, which is obtained from the tracking. The sum is over all instrumented cells in the three calorimeter modules. The radial weights $W_k(R)$ are determined by linear interpolation between a set of radial weights $W_k(R_k)$ which are fitted at discrete distances R_k, where $k \in (1,\cdots,N)$:

$$W_k(R) = \begin{cases} W_1 & \text{if } R < R_1 \\ W_N & \text{if } R > R_N \\ W_k \times \frac{R_{k+1}-R}{R_{k+1}-R_k} + W_{k+1} \times \frac{R-R_k}{R_{k+1}-R_k} & \text{otherwise} \end{cases}$$

In this study, $N = 16$ for each module (steps of 1 cm), providing a total of 48 free parameters. The radial weights for each module, at each energy point, were obtained by minimizing the resolution of the reconstructed energy. These fits are done separately at each beam energy, providing a set of weights for each sample. These are shown for each module in figure 23 for energies from 120-200 GeV; the observed energy dependence is not dramatic. Reconstructions using the 120 GeV weights, the 200 GeV weights and the average of the 120, 150 and 200 GeV weights yield almost identical results for the energy resolution. The results presented in this section were obtained using the 200 GeV weights.

The weight distributions in the three modules can be qualitatively understood as follows: in the FCal1, the energy deposition at small radius is dominated by the electromagnetic core of the shower, so the weights in this region are expected to be about 1. As one moves into the halo of the shower, the hadronic component becomes larger and the weights rise correspondingly. At higher

2008 JINST 3 P02002

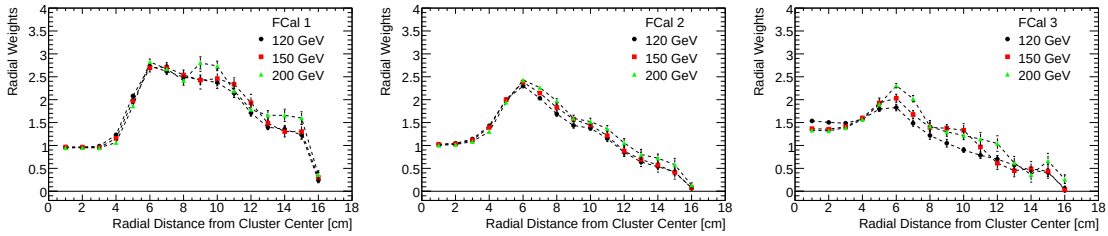

Figure 23. Radial weights for the three FCal modules, shown for energies from 60 to 200 GeV, derived from the beam test data.

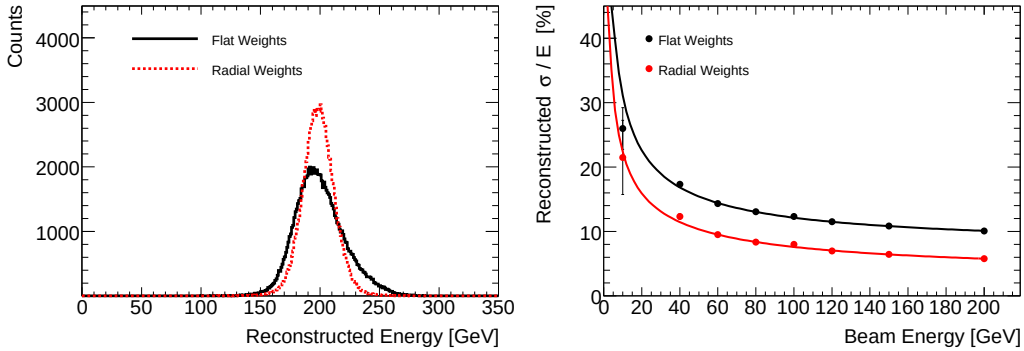

Figure 24. The plot on the left shows the reconstructed energy for 200 GeV data taken at the 4L position, obtained using radial weights. The plot on the right shows the resolution obtained with the radial-weighting technique. In each case, the result is displayed with the equivalent results from the flat-weighted reconstruction technique.

radius still one begins to move away from the region in which there are significant energy deposits, and the weights fall to small values, providing for the suppression of channels contributing mainly noise. Note that this procedure can be applied without clustering, since weights tend to zero as one moves far from the shower axis. In the FCal2 module the overall shape is similar to that of the FCal1 though fall-off begins more rapidly due the denser absorber. In the FCal3 where most of the deposited energy is hadronic, and where any EM component does not necessarily appear at the shower centre, the weights begin at values larger than 1. Note that, in the analysis presented here, distances were calculated with respect to the geometric centre of the readout cell. This differs from the technique used in a past analysis [16] which took the distance to a cell as the average distance to its three closest electrodes. Furthermore, in the extraction of the radial weights, the beam-energy constraint was not applied. For both of these reasons, the radial weights derived here are not optimal, but the results are included to illustrate the performance that can be expected from a more sophisticated weighting procedure. The optimal implementation of this technique will be the subject of further study.

The results of this reconstruction, applied to the 200 GeV data sample, are shown in the left-hand plot of figure 24 along with the equivalent distribution from the reconstruction with flat weights. For the radial-weights reconstruction, the mean reconstructed energy is 198.8 GeV,

2008 JINST 3 P02002

slightly lower than 200 GeV due to the absence of the beam-energy constraint in the weights determination. Reconstruction using the 200 GeV flat weights yields a mean reconstructed energy of 200 GeV, though the peak is at a slightly lower value due to the asymmetric shape. The improvement in the energy resolution, using the radial weighting, is apparent. The resolution as a function of energy is shown in the right-hand plot of figure 24 and compared with the results from the reconstruction with flat weighting. The stochastic term is reduced from 94% to about 70%. The fitted constant term is $(3.0 \pm 0.5)\%$. The resolution at 200 GeV is improved from 10.1% to 5.8%.

5. Summary and conclusions

The FCal detector for one side of ATLAS has been tested with electron and hadron beams in the energy region of about 10-200 GeV. Analysis of the beam test data shows that the FCal performance meets the ATLAS requirements. Further analysis is underway to look at the FCal response for particles that hit the detector at high values of $|\eta|$, near the edge of the FCal acceptance, and to investigate the change in performance when upstream material is added to simulate conditions at ATLAS.

Due to scheduling difficulties, the final ATLAS LAr warm electronics were unavailable for the beam test. The gains in the final electronics are different from those of the prototype electronics that were used, but these gain differences are reasonably well understood and more detailed determination is on-going. Because the predicted energy response agrees, with reasonable precision, with the measured response, we are confident that application of the calibrations constants (ADC/MeV) with the gain ratios will give an acceptable calibration for initial data-taking with the final electronics.

The noise contribution in a single FCal readout channel is dominated by irreducible, incoherent kT noise in the preamplifiers. A first-principles calculation of the noise seen after the shaper agrees with observations. Measurements show that about 10% of the total noise in a single channel is coherent noise, in line with the specifications for the prototype ATLAS electronics used in the beam test. For the final ATLAS front-end electronics, that specification was tightened to 5%.

Because the sampling fraction of the FCal modules is very small, the stochastic term is dominated by shower fluctuations. It dominates the energy resolution only over a relatively narrow range of energies, with the noise and constant terms dominating at low and high energies, respectively [6]. The constant term is dominated by the variation in the response as a function of transverse position. For showers which develop near the gap of an electrode, the response is larger than for showers which develop near the middle of an electrode rod or between electrodes. To the precision of the beam profile chambers we have mapped this response variation in the transverse direction. Correcting for this transverse response variation can significantly reduce the constant term. However, in ATLAS there are no tracking chambers upstream of the FCal and pileup noise will hamper attempts to determine the transverse position via shower-sharing between neighbouring readout channels to the required accuracy. For these reasons, none of the results reported here include such corrections.

The E_T resolution requirement for the FCal is specified as $\Delta E_T/E_T < 10\%$ for $E_T > 25$ GeV. In the case that the position resolution (and therefore the angular resolution) is perfect, this translates to an energy resolution specification of $\Delta E/E < 10\%$ for $E > 250$ GeV at $|\eta| = 3.0$ and for $E > 1000$ GeV at $|\eta| = 4.4$. In the beam test, the position of particles can be determined by shower

2008 JINST 3 P02002

sharing to a precision of 1 mm or better [14]. Pileup will degrade this precision. Assuming a precision of 7.5 mm, the angular resolution would be $\Delta\theta/\theta = 1.5\%$ at $|\eta| = 3.0$ and $\Delta\theta/\theta = 6.0\%$ at $|\eta| = 4.4$ requiring an energy resolution of $\Delta E/E < 9.9\%$ at $|\eta| = 3.0$ and $\Delta E/E < 8\%$ at $|\eta| = 4.4$. The results presented here show that the performance of the FCal exceeds these requirements.

While the rms energy resolution is an important parameter characterizing the performance of a calorimeter, the tails of the energy resolution function are also important. For instance, suppose a 200 GeV hadron strikes the forward calorimeter. What is the probability that the calorimeter response exceeds 300 GeV or falls below 100 GeV? Such rare occurrences will lead to an instrumental missing E_T signal. In a good calorimeter the probability of this occurrence should be well below the expected physics signal. In the case of the ATLAS FCal, in the energy spectrum reconstructed from the 200 GeV sample, we find the probability that a beam particle gives a measured response above 300 GeV to be $(0.024 \pm 0.005)\%$. The probability to have a measured response below 100 GeV is $(0.052 \pm 0.007)\%$, with about 90% of such events being consistent with late showering particles that are not fully contained, and about half of the remainder being attributed to muons.

6. Acknowledgments

The support of the CERN staff operating the SPS and the H6 beam line, in particular the frequent assistance of Ilias Efthymiopoulos and Adrian Fabich, is gratefully acknowledged. We thank Jens Spanggaard for his help with the CEDAR. We would also like to thank our colleagues from the ATLAS Liquid Argon Electronics and Cryogenics groups for their invaluable help, with particular thanks to Francesco Lanni and Michael Rijssenbeek. We additionally thank the following people for their contributions: Sing-Leung Cheung, Teresa Embry, Philippe Gravelle, Mohammad Hamidian, Adam Hincks, Liz Inrig, Michael Starr, Kevin Sung, Peter Thompson, Dan Tompkins, Kenneth Vincent and Manuella Vincter.

This work has been supported by the US Department of Energy (DOE DE-FG02-04ER41298), the Natural Science and Engineering Research Council of Canada, the Russian Federal Agency for Atomic Energy and the Russian Federal Ministry of Education and Science

References

[1] ATLAS collaboration, *ATLAS letter of intent*, CERN-LHCC-92-4 (1992).

[2] ATLAS collaboration, *ATLAS technical proposal*, CERN-LHCC-94-43 (1994).

[3] ALEPH, DELPHI, L3 and OPAL collaborations, *Search for the standard model Higgs boson at LEP*, *Phys. Lett.* **B 565** (2003) 61.

[4] S. Baranov et al., *ATLAS radiation background task force summary document*, ATL-GEN-2005-001 (2005).

[5] ATLAS collaboration, *ATLAS liquid argon calorimeter: technical design report*, CERN/LHCC/96-41 (1996).

[6] J.C. Armitage et al., *Electron signals in the Forward Calorimeter prototype for ATLAS*, 2007 *JINST* **2** P11001.

[7] C. Bovet et al., *The CEDAR counters for particle identification in the SPS secondary beams: a description and an operation manual*, CERN Yellow Report 82-13 (1982).

2008 JINST 3 P02002

[8] www.iseg-hv.com.

[9] ATLAS Liquid Argon EMEC/HEC collaboration, C. Cojocaru et al., *Hadronic calibration of the ATLAS liquid argon end-cap calorimeter in the pseudorapidity region* $1.6 < |\eta| < 1.8$ *in beam tests*, *Nucl. Instrum. Meth.* **A 531** (2004) 481 [physics/0407009].

[10] ATLAS Electromagnetic Liquid Argon Calorimeter group, B. Aubert et al., *Performance of the ATLAS electromagnetic end-cap module*-0, *Nucl. Instrum. Meth.* **A 500** (2003) 178.

[11] F. Hubaut et al., *Implementation of a serial protocol for the liquid argon calorimeters of ATLAS*, *IEEE Trans. Nucl. Sci.* **48** (2001) 1254.

[12] CHORUS collaboration, M.G. van Beuzekom et al., *The trigger system of the CHORUS experiment*, *Nucl. Instrum. Meth.* **A 427** (1999) 587.

[13] R. Gurin and A. Maslennikov, *ControlHost distributed data handling package, User manual, CASPUR program library note C001*, Rome Italy (1995), http://www.nikhef.nl/~rudd/HTML/choo_manual.html.

[14] A. Savine et al., *Position measurements and response uniformity of the LAr FCal prototype for ATLAS*, Proceedings of the 7$^{\text{th}}$ International Conference on Calorimetry in High Energy Physics, Ed. E. Cheu et al., World Scientific (1998).

[15] W.E. Cleland and E.G. Stern, *Signal processing considerations for liquid ionization calorimeters in a high rate environment*, *Nucl. Instrum. Meth.* **A 338** (1994) 467.

[16] A. Savine, *Hadronic energy resolution improvement in calorimeter with fine transverse segmentation*, Proceedings of the 9$^{\text{th}}$ International Conference on Calorimetry in High Energy Physics, Ed. B. Aubert et al., Frascati Physics Series (2000).

2008 JINST 3 P02002